CROSSED-FIELD AMPLIFIER

Crossed-field amplifiers (CFAs) are well suited to the amplification of high peak powers and today find their major application in radar system transmitters. Gain is relatively low (about 10–13 dB) but efficiency is high (40–60%). Voltage, size, and weight are significantly less than for traveling-wave tubes at the same output power level. A common configuration in present radar systems is a high-gain traveling-wave tube (TWT) driving a final stage CFA.

CFAs employ radiofrequency (RF) interaction between a wave propagating on a slow wave structure and electrons traveling in crossed (i.e., perpendicular) dc electric and mag-

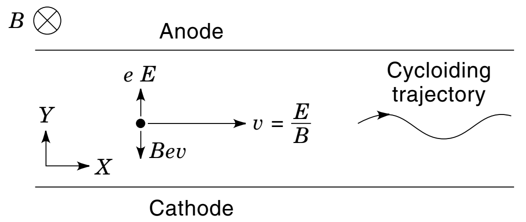

Figure 1. Basic motion of electrons in crossed dc electric and magnetic fields. Motions are shown in the laboratory frame of reference.

netic fields. Figure 1 shows the basic dc geometry governing electron flow. A dc voltage is applied between a pair of electrodes, and a magnetic field is applied perpendicular to the electric field. The term *sole* for the negative electrode in Fig. 1 has been adapted from French usage—much of the early work on one variant of this device was done in France in the 1950s. In Fig. 1 there is an electric field force in the $+y$-direction resulting from the applied voltage and a magnetic field force in the $-y$-direction resulting from the electron velocity in the x-direction and the magnetic field. For a velocity equal to E/B (electric field/magnetic field) these forces balance. An electron injected into the system at this velocity will continue to travel smoothly. More generally, electrons injected at other velocities will oscillate about the smooth trajectory but will travel in the x-direction with an average velocity equal to E/B. This velocity is commonly referred to as the "drift velocity" or "guiding center" velocity. The smooth trajectory is called the "guiding center trajectory" and the oscillations around the smooth trajectory are called "cycloids" (from their mathematical form).

Figure 2 shows an RF wave propagating on a slow wave structure embedded into the anode surface and added to the system of Fig. 1. The fields shown represent the fundamental component of RF electric field. Details of the anode structure are left out. This field pattern propagates in the $+x$-direction at the phase velocity of the anode circuit wave. If the electric and magnetic fields are adjusted to make the electron drift velocity equal to the wave phase velocity, a cumulative interaction takes place. Figure 2 shows the motion of electrons released into this system. The motions are shown in a frame of reference traveling at the velocity of the RF circuit wave. In this reference frame, the guiding center trajectories are perpendicular to both RF electric and dc magnetic fields and have a guiding center velocity equal to E_{rf}/B. In general, there are cycloiding motions about the guiding center trajectory. The trajectories move toward the anode and toward the center of the decelerating phase of the RF wave. If the RF wave field is strong, electron motions are controlled by it and the motions shown in Fig. 2 persist over a range of E_{dc}/B drift velocities of the electrons.

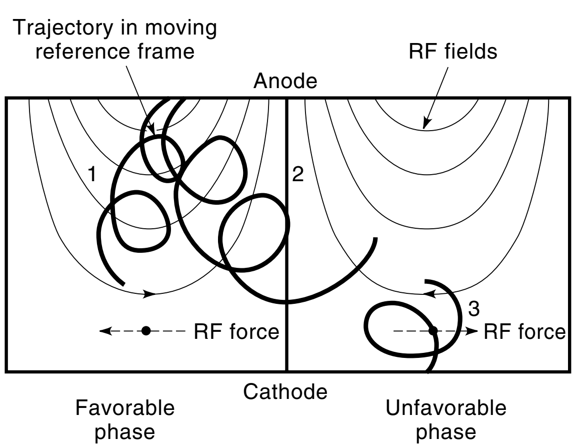

Figure 2. Basic motion of electrons when an RF wave propagating on the anode is added to the dc fields. The motions are now shown in a frame of reference moving in synchronism with the RF wave. In this reference frame the RF fields are stationary and the electron motions are relative to the field. The general nature of the motion is cycloiding (loops) around a guiding center of the trajectory which is perpendicular to the RF fields. The favorable phase of the wave is the one in which the x-directed component of the RF field retards the electrons and extracts energy from them. A trajectory (1) starting in this phase moves directly to the anode. A trajectory starting off of the center of the unfavorable phase (2) moves along the guiding center into the favorable phase and to the anode. A trajectory starting near the center of the unfavorable phase (3) extracts energy from the wave and moves to the sole.

As electrons in Fig. 2 move toward the anode, they continuously gain energy from the dc field. At the same time the electrons are, on average, decelerated by the RF field and give up energy to it, thus amplifying the wave. The transfer of energy to the wave can be analyzed in detail by examining the currents induced in the anode circuit by the electrons. Electrons strike the anode with a velocity only slightly greater than the average E_{dc}/B drift velocity. The energy they have gained from the dc field by traveling from their original position to the anode is converted to RF energy. This energy can be several times the energy dissipated on the anode by electron collection. A more detailed description of this CFA energy conversion is given in the last section of this paper.

CFA GEOMETRY

The crossed-field interaction can be incorporated into a device in two basically different ways. The first approach is to inject a sheet beam of electrons from one end between the plates of Figs. 1 and 2. This type of device is known as an "injected beam" CFA. The second approach is to make the sole a source of the electrons. The geometry and interaction then become similar to that of a magnetron. Such devices are known as "distributed emission" or "emitting sole" CFAs. Effort on injected beam CFAs was started in France in the 1950s and subsequently continued in the United States. High peak power injected beam CFAs for radar applications as well as continuous wave (CW) or high duty cycle injected beam CFAs for Doppler radar or countermeasures were developed. Although there has been a significant amount of effort on these devices, they now find little application, having lost out largely on the basis of cost effectiveness to either TWTs or emitting sole CFAs. Emitting sole CFA development started in the United States in the early 1950s through modification of high-power magnetrons. These devices are now employed in a number of radar systems.

Injected Beam CFAs

Figure 3 is a schematic diagram of an injected beam CFA. A sheet beam is formed in a crossed-field electron gun and injected between a nonemitting sole electrode and an anode incorporating a slow wave circuit on its surface. As amplification proceeds, electrons located in the wave phase in which

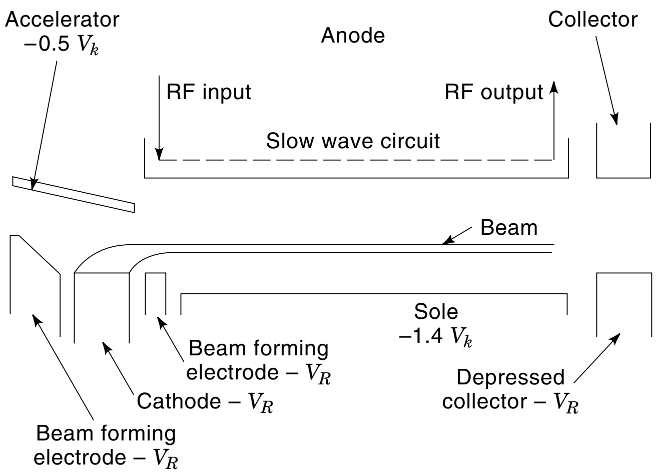

Figure 3. Schematic drawing of an injected beam CFA. The anode circuit is at ground potential and the cathode is operated negative with respect to ground.

they are decelerated by the RF wave (favorably phased electrons) move from the initial beam injection location toward the anode. Electrons in the wave phase in which they are accelerated by the wave (unfavorably phased electrons) move toward the site. Injected beam CFAs have a small sequel regime in which electrons are displaced from their original position but do not reach the anode circuit before entering the collector region. At high input signal levels, the electrons in the favorable phase as well as electrons from the edges of the unfavorable phase which are focused into the favorable phase are collected on the anode slow wave circuit. The circuit—and, in particular, the output portion of the circuit—must be capable of significant thermal dissipation. Stopping the interaction prior to the electrons reaching the anode is not practical because efficiency would then be greatly reduced. Electrons centered in the unfavorable phase move away from the anode and may not have been phase focused into the favorable phase by the end of the circuit. These electrons are collected in the collector region following the interaction region. Frequently a depressed collector at cathode potential and a second collector at anode potential are used. Unfavorably phased electrons that have gained energy from the RF wave are collected on the depressed collector. Electrons between cathode and anode are collected on the anode potential collector. Some injected beam CFAs are stable in the absence of RF drive. When this is the case, electrons reach the collector when no drive is present and are switched to collection on the slow wave circuit in the presence of RF drive.

Injected beam CFAs can be operated with a dc cathode voltage and with the beam pulsed either by pulsing the gun accelerator or a control grid over the cathode. The total power supply required is relatively complex, with floating sole, accelerator, and grid voltages required. Crowbar protection of gun elements is required. The complexity of injected beam CFAs and of their power supplies together with life limits imposed by relatively high cathode current densities has adversely affected the cost effectiveness of these devices and limited their applicability.

Emitting Sole CFAs

When the sole becomes the source of electron emission, a sheath of charge forms above the cathode surface, as shown in Fig. 4. Within this sheath electrons execute flat loops known as Slater trajectories. A lower-energy solution with sheath trajectories parallel to the cathode exists (Brillouin sheath) and it has been argued that the sheath trajectories should settle to this state. However, computer simulations of high power CFAs show that electrons are swept out of the interaction space too rapidly for this settling to occur and we obtain, instead, the trajectories in Fig. 4. The dc electric field in the sheath tapers from a value close to the space charge free value at the sheath surface to almost zero at the cathode surface. The reduction of dc field in the sheath reduces the average E_{dc}/B drift velocity of sheath electrons below that of electrons in the high field region above the sheath. Figure 5 shows the space charge distribution when RF fields are added to Fig. 4. The figure shows one wavelength of the interaction in a frame of reference moving in synchronism with the RF wave. The sheath electrons drift backward in this frame of reference. As they do so, they are slowed further by the RF wave fields and some of them are drawn into the high dc electric field region above the sheath. In this region, they are speeded up to synchronism with the wave and are formed by the wave fields into a spoke of charge extending upward toward the anode. As electrons flow through the spoke, they gain energy from the dc field and impart this energy to the RF field. The energy exchange mechanism is similar to that in the injected beam CFA but there is no small signal regime because large RF fields are required to capture the nonsynchronous sheath electrons and draw them up into the spokes. Large RF fields are further required to maintain the spokes centered in the favorable phase of the RF circuit wave. Emit-

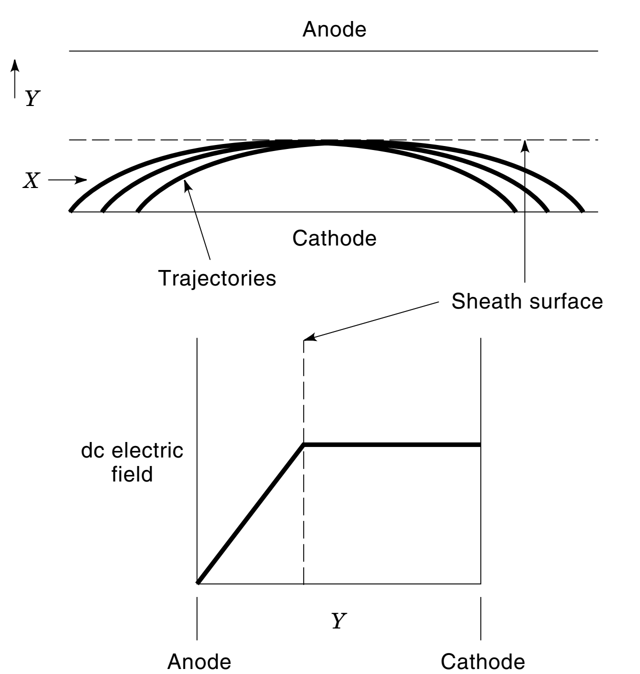

Figure 4. Trajectories of electrons released from an emitting sole (cathode) in the absence of an RF wave. The trajectories are shown in the laboratory frame of reference. A sheath of charge builds up above the cathode surface. Within the sheath, electrons execute long, flat trajectories having about half the height of a space charge free cycloid. The dc field is reduced in the sheath by the presence of the sheath space charge and approaches zero at the cathode surface.

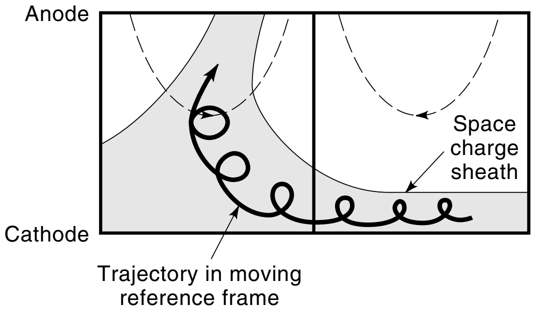

Figure 5. Space charge distribution and electron motions in the emitting sole geometry when RF fields are present. The sketch represents one wavelength of the interaction in a frame of reference moving in synchronism with the RF wave. The sheath surface is stabilized by the presence of the RF wave. A spoke of charge extends upward from the sheath to the anode in the favorable phase of the wave. Within the sheath, the reduction of the dc field results in an E/B drift velocity less than that of the anode wave. In the moving frame of reference, these sheath electrons drift backward. As they cross underneath the spoke, some of them are captured by the RF fields and are drawn into the spoke and up to the anode.

ting sole CFAs thus require the presence of an RF input signal of sufficient magnitude to control the space charge. In the absence of such a signal, they either oscillate or generate broadband noise. Once adequate input signal power is provided, the output power depends only to a small extent on the input power. Gain is limited by the necessity to provide an input signal strong enough to control the space charge. Typical gains of emitting sole CFAs in use today range from 10 to 18 dB.

There are several types of emitting sole CFAs depending on the nature of the anode slow wave circuit and on whether electrons are allowed to recirculate between output and input of the device. The simplest of these to understand, though not historically the first, is the forward wave emitting sole CFA described in the next section.

Forward Wave Emitting Sole CFA. Figure 6 is a schematic drawing of a forward wave emitting sole CFA. The interaction space in Fig. 5 is wrapped into a circle and electrons are allowed to recirculate from output to input. The slow wave circuit on the anode is of the forward wave type—that is, group (energy propagation) velocity and phase velocity are in the

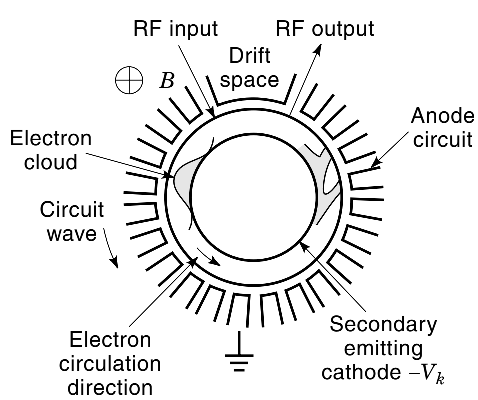

Figure 6. Schematic drawing of a forward wave emitting sole CFA.

same direction. The anode circuit is typically 15 to 20 wavelengths long, and there is one spoke of the type shown in Fig. 5 in each wavelength. The spokes are relatively diffuse near the input of the CFA but become sharply defined near the output. The space charge recirculates from output to input through a drift space free of RF fields. The spokes tumble forward and become partially debunched in this region. This debunching, together with the ability of the space charge fields at the input to reorganize the space charge, results in relatively small RF feedback from output to input via the recirculating space charge.

On the average, electrons gain energy from the dc field and lose energy to the RF field. However, the RF fields of the anode wave and local space charge field fluctuations within the sheath space charge cause some of the sheath electrons to gain energy from the RF fields rather than to lose it. These electrons strike the cathode and are quickly removed from the interaction space. They are thus prevented from detracting significantly from the RF gain contributed by electrons that give up energy. The electrons striking the cathode cause secondary emission electrons to be generated at the cathode surface. If the secondary emission yield of the cathode is greater than unity, the electron emission can be supplied entirely by secondary emission. Many emitting sole CFAs have cathodes that can supply only secondary emission and are operated cold. Beryllium and platinum are such secondary emitting surfaces. Other emitting sole CFAs use tungsten matrix dispenser cathodes, which are capable of supplying thermionic emission but are operated at temperatures low enough so that the thermionic component of the emission is small. Dispenser cathodes and platinum secondary emitters are operated in high vacuum. Beryllium secondary emitters require a small pressure of oxygen (e.g., 10^{-7} Torr) to maintain their secondary emission yield. The bombardment of the cathode by electrons that have gained energy results in power dissipated on the cathode. Typically about 10% of the dc input power appears as cathode bombardment. To dissipate this power, some emitting sole CFAs use liquid cooled cathodes.

Most of the current emitted by the cathode is returned to it and only a portion enters the spokes and reaches the anode. The division between anode current and current returned to the cathode depends on cathode emission conditions and is typically about one quarter to the anode and three quarters to the cathode. The cathode emitted current density is, therefore, about four times the anode current divided by the cathode area. This current density can become very high. However, for secondary emitters, current density is not the limit it is for thermionic emitters. Secondary emitters can give current densities of thousands of amperes per square centimeter if the primary current density is correspondingly high. Life of secondary emitters is not dependent on current density, as is the case for thermionic emitters. Cathode life considerations for emitting sole CFAs are thus completely different than they are for microwave tubes using thermionic emitters. Secondary emitting cathodes have the potential for unlimited life. To date, life in excess of 50,000 hours has been obtained in some CFAs. It must be noted that in very low power CFAs the energy of electrons striking the cathode may not be enough to produce greater than unity secondary emission yield. Such CFAs require thermionic emitters and are subject to the life limitations of such emitters.

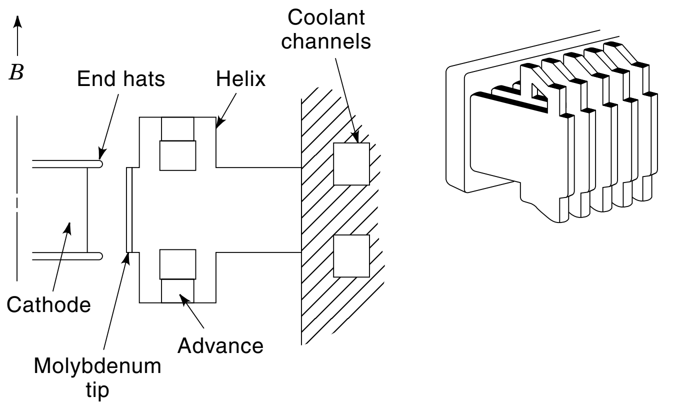

Figure 7. A helix coupled-vane forward wave slow wave circuit used in CFAs. The circuit is fabricated from copper, which has a high thermal conductivity. The molybdenum tip absorbs the transient temperature rise during an RF pulse. The end hats confine the space charge axially.

An emitting sole CFA using a cold secondary emitting cathode will turn on when RF drive and the cathode voltage are applied. A small amount of charge is generated by the RF and dc voltages—possibly by field emission from the cathode or from the anode structure. The initial charge generation process is poorly understood at this time. The initial charge is multiplied by multiple strikes of electrons on the secondary emitting cathode. Charge thus builds up and the CFA turns on. The buildup time can be a few nanoseconds. There is, however, a variable delay in the development of initial charge that can result in a jitter of tens of nanoseconds in the turn-on time for the first pulse in a train of pulses, such as is used in a radar transmitter. Once a CFA has started amplification of a pulse train, some charge is left in the interaction space at the end of each pulse and can be used to start the next pulse. Persistence of such charge for 10 to 20 ms has been observed. Low starting jitter is thus observed for pulse repetition rates down to about 50 Hz.

A number of different types of anode slow wave circuits have been employed. Figure 7 shows one example of such a circuit known as a double-helix coupled vane circuit. Radial vanes are coupled by helices mounted on the top and bottom of the vanes. The circuit is fabricated using a series of brazing and subassembly machining steps. The helices can be viewed as wrapped-up strip lines and the vanes as shunt stubs to ground. The resulting structure is a passband filter. The phase velocity of the wave as well as the strength of the RF field varies with frequency. Only a portion of the passband of the filter is useful for the interaction. CFAs using circuits of the kind shown in Fig. 7 typically have operating bandwidths of 10 to 15%.

Figure 8 shows a photograph of an S-band forward wave CFA that utilizes the helix coupled vane circuit of Fig. 7. This CFA yields a peak power of 125 kW and an average power of 2 kW over a bandwidth of about 12%. The CFA operates using a pulsed cathode voltage of 13 kV. Efficiency is about 50% and gain is 12 dB. This CFA uses a liquid-cooled beryllium secondary emitting cathode. The cylindrical exterior shell around the CFA in the photograph is a soft iron return for the magnets inside the shell. This construction yields a magnetically shielded design. Weight of the complete CFA package is 55 lb.

Figure 8. Photograph of an *S*-band forward wave CFA.

Backward Wave Emitting Sole CFAs. The development of backward wave emitting sole CFAs preceded that of forward wave CFAs by several years. The original devices (Amplitrons) were realized by interrupting a strapped magnetron circuit and providing input and output ports. In backward wave interaction the direction of the wave phase velocity and the direction of energy flow (group velocity) are opposite.

Figure 9 shows a backward wave circuit used in *X* and Ku-band CFAs. The circuit is a stub-supported interdigital line. A wave can be visualized as propagating between the interdigital fingers, as shown by the dotted line. In addition to the phase advance of this wave, the interdigital finger geometry results in a reversal of the field direction in alternate gaps.

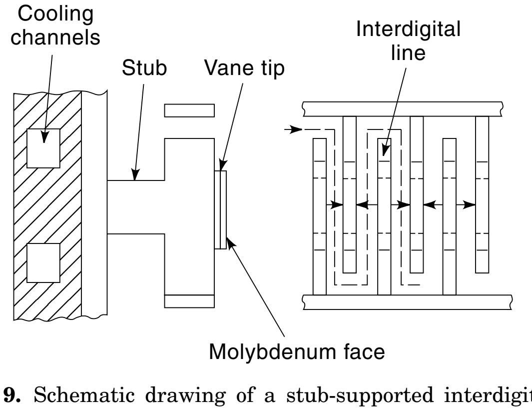

Figure 9. Schematic drawing of a stub-supported interdigital line slow wave circuit. An RF wave propagates along the meandering path between vanes indicated by the dotted line. The arrows in the gaps between vanes show the direction of the RF field at an instant of time assuming no phase advance of the wave (i.e., at the lower cutoff frequency). They illustrate the geometrical field reversal, which gives the circuit its backward wave characteristic.

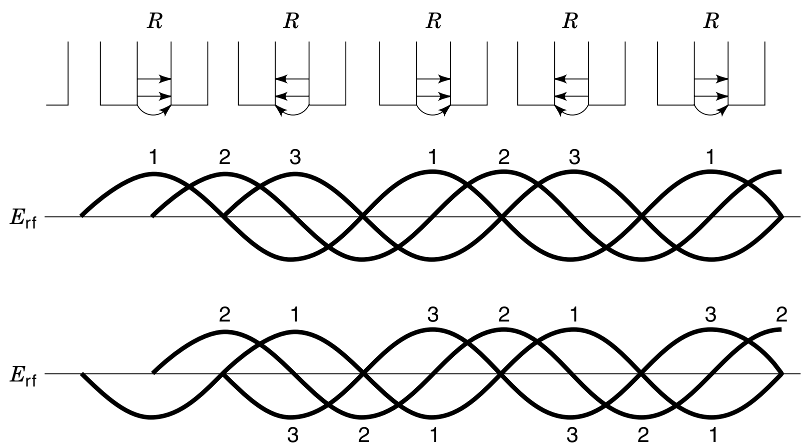

Figure 10. Top: Vane array showing field direction at time instant 1 for a forward wave circuit. Center: Magnitude of fundamental component of circumferential E-field for forward wave at three successive time increments separated by one quarter period. In a backward wave circuit the field direction is reversed in alternate gaps (R). The fields in the center are thereby converted to those shown on the bottom. The result is a field pattern propagating to the left.

This reversal is indicated in the figure at the low-frequency cutoff at which there is no phase advance along the dotted path.

Figure 10 illustrates the difference between forward and backward waves. A series of vane gaps is shown at the top of the figure, with the rf field directions indicated for a wave propagating to the right with a phase shift per section of 90°. The fields are drawn for an instant in time at which the fields are a maximum in one set of gaps and zero in the alternate gaps. Consider first the case of a forward wave circuit of the kind shown in Fig. 7. The set of waveforms in the center of the figure represents the amplitude of the fundamental space harmonic component of circumferential RF electric field midway between cathode and anode. Wave 1 represents the fields resulting from the gap fields at the top of the figure. Waves 2 and 3 represent the fields at successive instants of time separated by one quarter RF cycle. The field patterns on the circuit move to the right in same direction as the wave propagation. A positive field retards electrons and is thus the wave phase in which the electrons must be bunched for interaction. If the wave and the electrons move to the right from the center of one gap to the center of the next gap in the same time, the normal synchronous forward wave interaction occurs.

In the backward wave circuit of Fig. 9, the field reversal in alternate gaps changes the waveforms shown in the middle of Fig. 10 to those shown on the bottom of Fig. 10. The wave on the circuit continues to propagate to the right (the direction of energy propagation) but the direction of the fields is reversed in the alternate gaps. Suppose at time instant 1, the fields are reversed in the set of gaps (labeled R) at the top in which the fields are a maximum. The field in the interaction space will be reversed for time instant 1, as shown at the bottom of the figure. When the wave on the circuit propagates to the right by one period, the fields are not reversed. The field for time instant 2 is thus the same as in the center of the figure. For time instant 3, the fields are again reversed. Although the energy on the circuit is propagating to the right, the fundamental space harmonic component of the fields in the space between cathode and anode represent a wave with a phase velocity propagating to the left. To obtain cumulative interaction with this wave, the electron flow must be to the left and synchronous with this wave. Figure 10 has been drawn for a phase shift of 90° per circuit section, which makes the fields and the resulting waves easier to visualize, but the principles of interaction with forward and backward wave circuits hold independent of the phase shift per section.

Figure 11 is a schematic of a backward wave CFA. This figure should be compared with Fig. 6 for a forward wave CFA. The direction of electron circulation is reversed relative to the RF input and output ports, which are interchanged from their position in Fig. 6. Power still grows in the direction from input to output—the direction of the wave's energy flow. The space charge now recirculates through the drift space from input to output. Backward wave CFAs may use a drift space and debunching of the space charge, as is done in forward wave CFAs. Alternately, some backward wave CFAs (amplitrons) use a short drift space and utilize the rf feedback resulting from the recirculated bunched charge to enhance gain.

Figure 12 shows a photograph of an X-band CFA that utilizes the stub-supported interdigital line circuit. This CFA yields 1 MW peak and 1 kW average power over a 5.5% bandwidth. The CFA is operated from a pulsed cathode voltage of 13 kV. This CFA employs a tungsten matrix dispenser cathode heated by electron bombardment of the cathode. No heater is required. Efficiency is about 45% and gain is 13 dB. This CFA uses external horseshoe magnets, which are clearly visible in the photograph. The weight of the CFA with magnets is 32 lb.

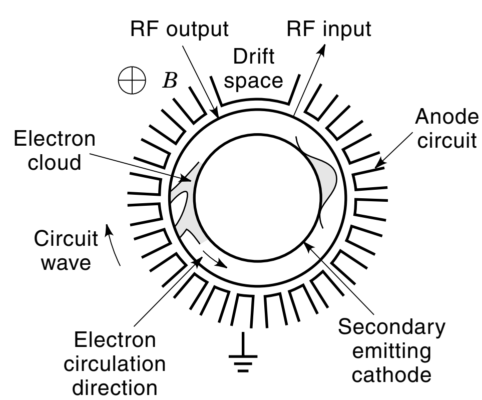

Figure 11. Schematic drawing of a backward wave emitting sole CFA.

Figure 12. Photograph of an X-band backward wave CFA.

A fundamental property of backward wave circuits is that phase velocity must vary as a function of frequency. The percentage separation of the V–I curves over a given percentage bandwidth is greater than for a forward wave CFA. Backward wave CFAs, which must be tuned over their operating bandwidth, are therefore operated from a constant current or constant power (line type) modulator, which automatically adjusts the cathode voltage as the frequency is changed. The voltage adjustment occurs because of the internal impedance characteristic of the modulator. In one radar application the frequency of operation of a CFA similar to the one in Fig. 12 is swept over the full bandwidth of the CFA in about a microsecond.

CFA PERFORMANCE LIMITS

The peak output power of an emitting sole CFA is determined by the geometry of the interaction space and the cathode voltage:

$$P \sim V_0^2 (h/\lambda_o) N \tag{1}$$

where V_0 is the cathode voltage, h is the axial height of the circuit, λ_o is the free-space wavelength, and N is the number of circuit sections. The number of sections in existing CFAs has varied from 13 to about 80. The choice is restricted by the type of CFA. Regenerative CFAs (Amplitrons) that have a short drift space and substantial RF feedback as a consequence of the bunched recirculating charge operate satisfactorily with 13 to 17 sections. In the absence of strong regeneration, a larger number of sections is needed. A limit to the number of sections that can be usefully employed is imposed by circuit losses. Increasing the number of sections increases circuit losses and reduces efficiency. The parameter h/λ_o is limited to about 0.25 by the properties of slow wave circuits. It follows that the cathode voltage is a major determinant of the peak power. For 1 MW peak power output, voltages are in the range of 25 to 35 kV. For 100 kW peak output, voltages are in the range of 10 to 15 kV. The upper limit on peak output is set by voltage gradient limits. The dc gradient increases approximately proportional to the frequency and to the square root of voltage. For the kind of CFAs described previously, the limit in the X-band is a few megawatts. In the S-band it is 20 to 50 MW. The lower limit on usable peak output power for emitting sole CFAs is determined by the minimum practical circuit pitch. The pitch is proportional to the square root of voltage and becomes increasingly fine grained as the voltage is reduced. At the S-band, a 1 kW CW emitting sole CFA has been developed. At the X-band, the minimum usable peak power is about 20 kW. At frequencies above the Ku-band it becomes extremely difficult to fabricate the fine-grained circuits required. At frequencies above the C-band, backward wave CFAs are preferred because their circuits are easier to fabricate.

The average power of CFAs is determined by the thermal properties of the slow wave structure, which must dissipate the energy of the collected electrons. For vane-type structures such as shown in Fig. 11, the thermal impedance of the path through the vane to the coolant channel limits the allowable dissipation. This impedance is proportional to the frequency of the design. For vane-type circuits average power capability thus decreases linearly with frequency. The pitch of the circuit depends on the peak power (approximately fourth root of peak power). Higher peak power CFAs thus also have higher average power capability. An average power capability of about 2.0 kW is possible for a 1 MW peak power CFA in the X-band (1 kW is now available). In the S-band this increases to about 5 kW.

Both forward and backward wave circuits may be fabricated using bars coupled with straps (backward wave) or helices (forward wave). Average power capability is greatly increased when the circuit elements are hollow bars that may be liquid cooled. The conductive thermal impedance from the vane tip to the coolant is then greatly decreased, and the heat transfer from the metal bar to the coolant becomes the limiting thermal impedance. For a given flow rate of coolant, there is a maximum heat transfer density. Average power capability thus decreases as the square of the frequency. Using water or water/glycol coolant, a heat transfer density of 2 kW/cm^2 has been used in CFAs now in use. Local boiling of the water is required to achieve this high heat transfer density. Dielectric coolants yield much lower heat transfer densities. An average power of 10 kW at C-band and 50 kW at S-band in a megawatt peak power level CFA is feasible. Higher heat transfer densities have been obtained experimentally. A 500 kW CW S-band CFA was demonstrated in the 1960s. For frequencies above C-band, it is very difficult to fabricate a circuit using hollow bars. So far, hollow bar cooling has been restricted to C-band and below.

The pulse length limit of CFAs is determined by the transient heating of the anode surface during a pulse. During a pulse heat is dissipated in the surface of the vane tip faster than it can be conducted away and the vane tip temperature increases. Between pulses the temperature drops back to the average value. This high-rate thermal cycling can lead to a mechanical breakup of the anode surface. A refractory metal tip—usually molybdenum—is used to improve tolerance to this thermal cycling. The transient temperature rise of the vane tip is determined by the peak power dissipation density and the pulse length:

$$T \sim P/A\sqrt{t_p} \tag{2}$$

where T is the transient rise, P/A is the peak dissipation density, and t_p is the pulse length. For a fixed transient temperature rise, the maximum pulse length decreases as the fourth power of frequency. For a 1 MW peak power CFA in X-band, the maximum pulse length is about 2 μs. The limit increases rapidly at lower frequencies—to milliseconds in L-band.

THE PHYSICS OF RADIATION GENERATION IN CFAs

The fundamental mechanism of radiation generation is the same for all CFA designs. It is discussed here in some detail because it is destinctively different from other microwave devices. The process of energy conversion to radiation in a CFA is illustrated by considering the interaction of a single electron with the cavity fields. One can envision the electron orbit in the static fields as that of a point on spinning wheel rim. The center of the wheel ("guiding center") at Y streams along with the $u = c\boldsymbol{E}_o \times \boldsymbol{B}_o/B_o^2$ velocity while the electron is rotating about the GC at the cyclotron frequency $\Omega = eB_o/mc$ with radius $\rho = |\boldsymbol{v} - \boldsymbol{u}|/\Omega$, where v is the total velocity. The electron energy and momentum are then expressed solely in terms of the GC quantities:

$$\epsilon = \frac{1}{2}mu^2 + \frac{1}{2}m\Omega^2\rho^2 + eE_oY, \tag{3}$$

$$P = mu + m\Omega Y \tag{4}$$

where the second term in Eq. (4) is the canonical momentum of the vector potential from B_o. It turns out that the energy exchange with the cyclotron motion averages to zero over an rf period for the usual CFA operation frequencies. Also, the drift velocity u is fixed by the external fields. Hence the exchanged energy during the emission/absorption of a radiation quantum (caviton) equals just the change in the electrostatic energy of the electron GC:

$$\mp\hbar\omega = eE_o\delta Y = \delta(-e\Phi_o) \tag{5}$$

where $-e$ is the electron charge, E_o the electric field, and Φ_o the potential function. In a similar manner the change in the radiation momentum equals the change in the canonical momentum:

$$\mp\hbar k = m\Omega\delta Y = \delta(-eA_x/c) \tag{6}$$

stemming from the GC displacement across the vector potential $A_x = B_oY$. Dividing Eq. (5) by (6), one recovers the Buneman–Hartree (BH) condition for wave-particle resonance,

$$\omega - uk = 0 \tag{7}$$

where the drift velocity equals the wave phase velocity ω/k. Particle trapping due to finite RF amplitude and finite line width $\delta\omega = 1/Q$ allows operation in the vicinity of the resonant velocity. From either Eq. (5) or (6) it follows that the GC shift per emission or absorption is $\delta Y = \pm\Delta$, where

$$\Delta = \frac{\hbar k}{m\Omega} = \frac{\hbar\omega}{eE_o} \tag{8}$$

Though classical electromagnetic theory can also describe the device operation, the above "semiclassical" treatment makes transparent a characteristic difference between CFAs and the rest of microwave devices: The electron recoil is not opposite to the direction of radiation emission but orthogonal to it, across the anode–cathode space.

Stimulated emission in crossed E and B fields involves changes in the electrostatic and vector potential only. The kinematic energy and momentum remain invariant during the transition.

Whether emitted radiation is amplified depends on the relative strength between absorption and emission probabilities. An electron emitting radiation moves upward toward the region of increasing radiation strength $V_1(Y) = V_1 \sinh(kY)$, while an electron absorbing radiation moves downward toward a region of decreasing radiation strength. Since the stimulated emission/absorption probabilities are proportional to $V_1^2(Y)$, it turns out that the net radiation gain is proportional to the *gradient* of the radiation intensity dV_1^2/dY in the direction perpendicular to the emission. Indeed, assuming a monoenergetic sheet beam, where the guiding centers are injected at $Y = b$ and uniformly distributed in RF phase, the single pass gain over a cavity length L is

$$G \equiv \frac{\Delta P}{P_r} = \frac{eZI_b}{mu^2}\frac{\omega}{\Omega}\frac{1}{2}\frac{d}{dY}\left(\frac{\sinh^2(kY)}{\sinh^2(kD)}\right)_b \frac{\omega^2L^2}{u^2}\theta(\xi) \tag{9}$$

where I_b is the beam current and the circulating power in the resonator was expressed in terms of the impedance Z as $P_\tau = V_1^2/2Z$. The line shape function

$$\Theta(\xi) = \frac{\sin^2\xi}{\xi^2} \tag{10}$$

carries the gain dependence on the detuning $\zeta = (\omega - ku)L/2u$ from exact resonance and determines the half-width of the excited radiation spectrum $\Delta\omega = \pi u/L$.

Notice that the gain is *symmetric* around to resonance, contrasting the antisymmetric gain of most other radiation devices [free electron lasers (FELs), cyclotron masers, traveling-wave tubes (TWTs)], clystrons powered by streaming electron beams. The explanation lies in the "recoilless" emission. Since the kinetic energy does not change during the exchange of a radiation quantum, the electron absorption and emission probabilities are peaked at the same frequency; as we saw, the net radiation gain comes from the spatial gradient in the radiation intensity. In other devices that convert kinetic energy into radiation, the Compton electron recoil causes emission and absorption to peak at slightly different frequencies; thus the net gain there is proportional to the frequency gradient $d\Theta/d\omega$ of the line shape. It is also worth pointing out that the basic CFA theory is two dimensional since the transverse gradient of the intensity is essential to the interaction. A one-dimensional, uniform amplitude plain wave interaction, which suffices in most other devices, would give zero gain for a CFA.

The gain formula of Eq. (9) applies to small-amplitude situations where the electron excursions remain small and the changes in the charge distribution in space are neglected. At high-power operation, the electron orbits under the influence of the RF form tongues toward the anode; the space charge bunches in space into the characteristic spoke structure. The bunching generates a considerable RF component in the charge and current distribution in the *A-K* space, which in turn affects the dielectric response function and RF energy flux in the *A-K* space. It can be argued, however, that power flux stored in the spoke self-fields, however significant compared to the *A-K* flux in vacuum (no space charge), still remains much smaller than the power flux in the anode circuit. This is further supported by measurements of the phase pushing of the loaded cavity against the cold tube operation, finding that the space charge induced change in the real part of the frequency is small indeed. We therefore focus on the large signal gain, related to the imaginary part of the frequency.

A direct computation of the energy exchange integral over one spatial wavelength and over one RF period yields

$$\frac{d}{dx}\left(\frac{V_1^2}{2Z}\right) = \frac{1}{\lambda}\int_d^D dY E_o(Y) I_s(Y) \tag{11}$$

where $I_s(Y)$ is the current flowing through one spoke. The integral begins at the hub surface $Y = d$ since the subsynchronous hub, where the stratified flow velocity moves quickly away from synchronism, has a much small contribution to the energy exchange. Steady-state operation and incompressibility of the GC flow guaranties conservation of the current $I_s(Y) = I$ through any spoke cross section. If space charge effects are also neglected, $E_o(Y) = \text{const} = V_o/D$, the above expression yields the output power $P_o = P_i + \delta P$ where

$$\delta P = \delta\left(\frac{V_1^2}{2Z}\right) = V_o I_o \left(1 - \frac{d}{D}\right) \tag{12}$$

and $I_o = NI_s$ is the total anode current from $N = L/\lambda$ spokes. Thus the power converted to RF over a single pass equals a fraction $(D - d)/D$ of the dc power provided by the external source. The rest of the dc power goes into the $E \times B$ drift kinetic energy of the particle emitted from the cathode; that amount is not converted to radiation and is eventually dumped as heat when particles reach the anode. One now has only to compute the spoke current as a function of frequency, RF power, dc voltage, and geometry.

When the electron GC orbits are viewed in a frame drifting at the RF phase velocity, they form the streamline patterns shown in Fig. 13. In the synchronous frame the RF field appears frozen in time and the streamlines covering one wavelength follow the equipotentials of the total transformed electrostatic potential. Two families of orbits exist. Orbits with unrestricted particle motion toward the anode and orbits that oscillate in Y about some average position. The boundary curve separating the two families, marked by the heavy line, is a separatarix. The four different topologies shown represent typical patterns under various detunings from resonance, RF amplitude, and hub charge density. The heavy shaded area contains the orbits reaching the anode and forming the spoke pattern. The light shaded area contains orbits whose contribution to the energy exchange averages to zero. The width of the spoke current channel is determined by the two outermost streamlines originating at the hub and reaching the anode. As the RF amplitude changes along the tube there is transition between various topologies; these transitions are smooth in the sense that the spoke current does not develop gaps or jumps. Notice that while the hub charge does not contribute directly to the energy exchange, it nevertheless affects the streamline topology and thus the anode current.

In general, the detection of all the possible patterns during the signal evolution and a self-consistent solution of Eq. (11) requires codework, particularly in cases of emitting sole CFA, where a hub forms above the cathode. However, the situation is again simplified in the case of a low space charge sheet beam; neglecting space charge effects limits the possible topologies to only two and allows an easy calculation of the spoke current. The results from theoretical predictions of the saturation gain are plotted in Fig. 14 versus the experimental measurements. The experiment demonstrates the symmetry of the gain versus frequency detuning.

Even at high power, high space charge CFA operation near the synchronous voltage, the spoke current I_s turns out nearly independent of the topology details and equal to that at exact synchronism. Then, roughly speaking, I_s scales as the hub charge density σ, times the axial height h, times the wavelength λ, times the RF-induced upward drift velocity $\sim V_1/\lambda B_o$ across the hub, $\sigma h V_1/\lambda B_o$. Now given that σ is near the so-called Brillouin density $\sigma \sim B_o^2$, and that $B_o \sim V_o$ for given frequency and anode–cathode gap, one has $I_o = (L/\lambda)\, I_s \sim (N/\lambda) h V_o V_1$. Substituting I_o in Eq. (12) recovers the empirical scaling of Eq. (1), provided that the circuit impedance (and thus V_1 under given power) is held constant. While the space-charge effects break the gain symmetry around resonance, the CFAs operate both above and below the synchronous voltage.

Recent advancements in computer speed and memory size have made possible the simulation of CFA operation by following the exact orbits of individual particles in the RF fields. Each macroparticle represents a large number of actual electrons; the electric field collectively generated is self-consistently included in the total field driving their orbits. Particle locations and the field values on a numerical grid are updated on a time step basis. The time step and the grid cell size are much smaller than the time and space scales that one wishes to resolve. The number of macroparticles is sufficiently large to statistically represent the effects from the thermal velocity spreads as well as the complications from the nonlinear nature of the interactions. On the other hand, the macroparticle number is much smaller than the number of the actual electrons resulting in an increased numerical fluctuation level. A compromise is usually striken between the acceptable numerical noise floor and the computational time required.

The charge distribution obtained with the code MASK during the simulation of a typical CFA tube with secondary emitting cathode is shown in Fig. 15. The formation of charge spokes carrying current to the anode vanes is clearly visible; the number of spokes equals the number of wavelengths in the interaction space, proceeding counterclockwise from the RF input to the output. The macroparticles shown are color-coded according to their weight, i.e., the number of electrons being represented. Different weights result from the dependence of the secondary emission yield on the impact energy on the cathode. The increasing ability of particle codes to

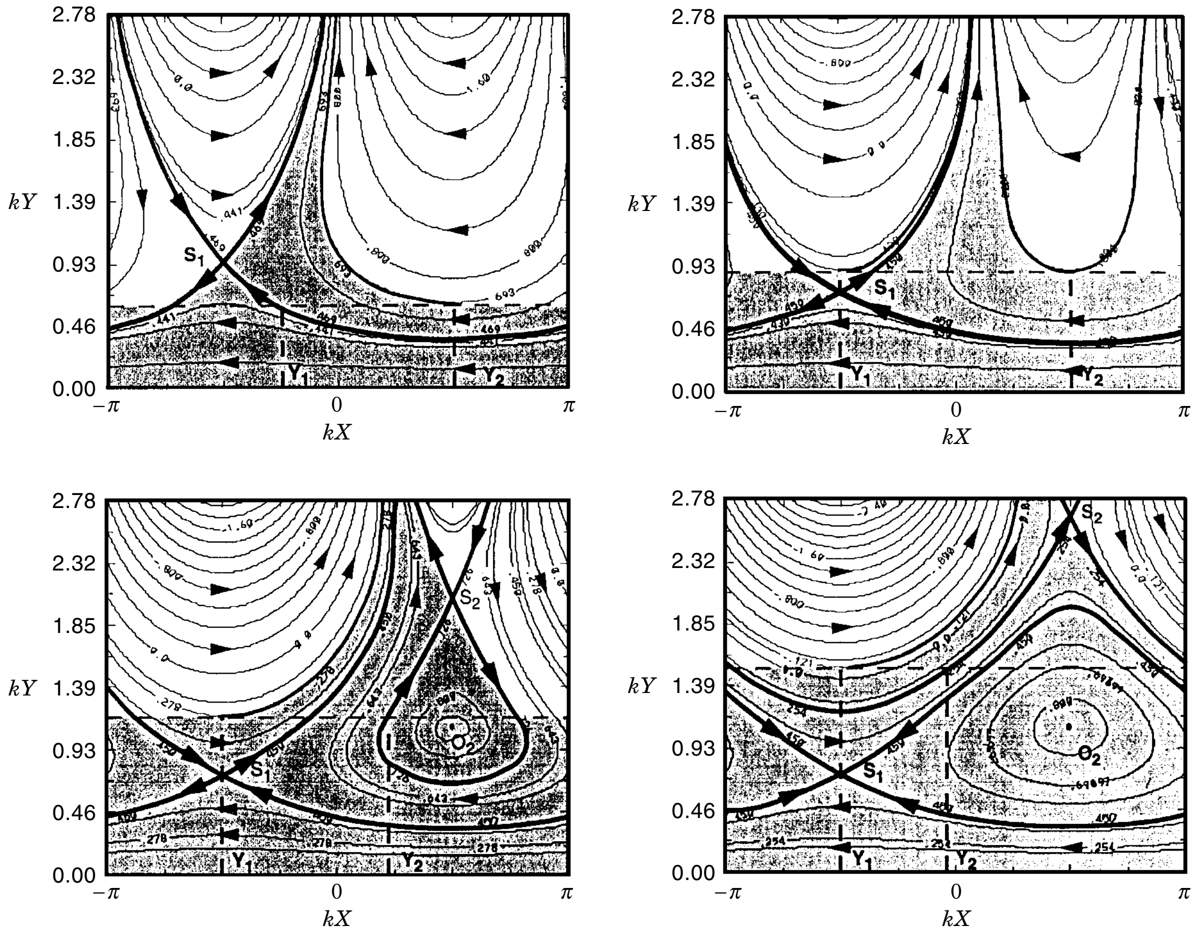

Figure 13. Some typical flow patterns forming within an RF wavelength $\lambda = 2\pi/k$ for various external voltage and space charge values. Arrows indicate the direction of the GC motion. The shaded area above the hub contains the orbits that reach the anode.

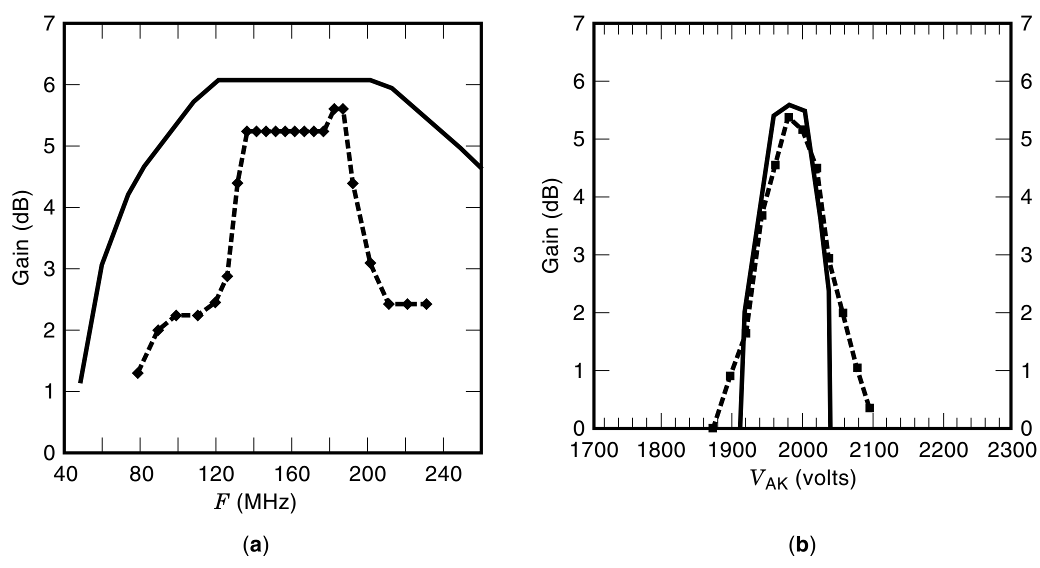

Figure 14. Gain versus detuning for an injected beam CFA, plotting theory (solid curve) versus experiment. (a) Gain versus frequency under fixed AK voltage in a linear format CFA. (b) Gain versus AK voltage under given frequency in a cylindrical CFA.

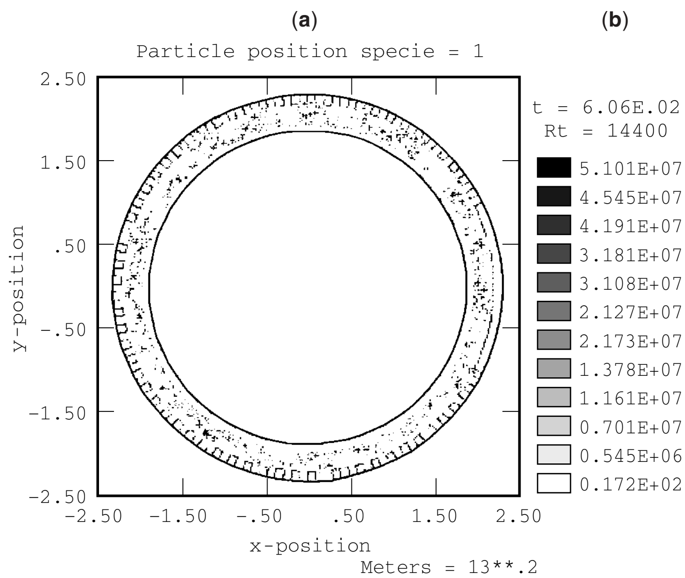

Figure 15. (a) Schematic of cross-sectional view of the space-charge distribution during steady-state CFA operation, obtained with computer simulation. The RF wave propagates counterclockwise. The spokes carrying current to the vane tips are clearly visible. (b) Chart indicating charge density, from min (bottom) to max (top).

mimic real-life operation conditions is steadily promoting their use as predicting tools in CFA design.

Reading List

A. S. Gilmour, *Microwave Tubes,* Norwood, MA: Artech House, 1986, Chapter 13. Excellent introductory treatment.

R. G. Hutter, *Beam and Wave Electronics in Microwave Tubes,* Princeton, NJ: Van Nostrand, 1960. This reference presents the derivation of the small signal gain of an injected beam CFA in a different manner than is described above.

E. Okress (ed.), *Crossed Field Microwave Devices,* New York: Academic Press, 1961. This reference contains many articles on the theory of injected beam and emitting sole crossed-field amplifiers and on the slow wave circuits used in such devices.

J. F. Skowron, The continuous cathode (emitting sole) crossed field amplifier, *Proc. IEEE,* **61**: 330–356, 1973. This reference is an excellent tutorial article describing the state of the art in 1973 and containing a useful bibliography of earlier work.

J. C. Slater, *Microwave Electronics,* New York: Van Nostrand, 1950. This reference describes the theoretical solutions for the space charge sheath.

The following references describe computer simulation of crossed-field amplifiers:

J. Browning et al., *IEEE Trans. Plasma Sci.,* **19**: 598, 1991.

D. P. Chernin, Computer simulation of low noise states in a high power crossed-field amplifier, *IEEE Trans. Electron Devices,* **43**: 2004, 1966.

G. Dombrowski, Simulations of magnetrons and crossed field amplifiers, *IEEE Trans. Electron Devices,* **35**: 2060, 1980.

J. Feinstein, in E. Okress (ed.), *Cross Field Microwave Devices,* New York: Academic Press, 1961, p. 554.

P. L. Kapitza, in D. ter Haar (ed.), *Collected Papers of P. L. Kapitza,* Vol. 2, New York: Pergamon, 1965, pp. 838–871.

H. L. McDowell, CFA computer modeling using a moving wavelength code, *Proc. 1st International Workshop on Crossed Field Devices,* University of Michigan, 1995.

R. McGregor et al., *IEEE Trans. Electron Devices* **41**: 1456, 1994.

S. Riyopoulos, Nonlinear self consistent theory for crossed field devices, *Phys. Rev. E,* **47** (4): 2839, 1993.

S. Riyopoulos, *Phys. Fluids,* **B3**: 3505, 1991.

S. Riyopoulos, *IEEE Trans. Plasma Sci.,* **20**: 360, 1992.

S. Riyopoulos, *Phys. Rev. E,* **47**: 2839, 1993.

S. Riyopoulos, *IEEE Trans. Plasma Sci.,* **22**: 626, 1994.

S. Riyopoulos, *IEEE J. Quantum Electron.,* **31**: 1579, 1995.

S. Riyopoulos, *Phys. Rev. E,* **51:** 4930, 1995.

S. Riyopoulos et al., *IEEE Trans. Electron Devices,* **39**: 1529, 1992.

S. P. Yu, G. P Kooyers, and O. Buneman, Time dependent computer analysis of electron-wave interaction in crossed fields, *J. Appl. Phys.,* **36** (8): 2550, 1965.

S. P. Yu, G. P. Kooyers, and O. Buneman, *J. Appl. Phys.* **36**: 2550, 1998.

Chung Chan
Northeastern University
Hunter L. McDowell
Communications and Power Industries
Spilios Riyopoulos
Science Application International Corporation

CROSS-SECTION, RADAR. See Radar cross-section.

CRTS, COLOR. See Cathode-ray tube displays